Abnormal glucose homeostasis in skeletal muscle–specific PGC-1α knockout mice reveals skeletal muscle–pancreatic β cell crosstalk

Christoph Handschin,[1,2] Cheol Soo Choi,[3] Sherry Chin,[1] Sheene Kim,[3] Dan Kawamori,[4] Amarnath J. Kurpad,[4] Nicole Neubauer,[4] Jiang Hu,[4] Vamsi K. Mootha,[5,6] Young-Bum Kim,[7] Rohit N. Kulkarni,[4] Gerald I. Shulman,[3] and Bruce M. Spiegelman[1]

[1]Dana-Farber Cancer Institute and Department of Cell Biology, Harvard Medical School, Boston, Massachusetts, USA. [2]Institute of Physiology and Zurich Center for Integrative Human Physiology, University of Zurich, Zurich, Switzerland. [3]Howard Hughes Medical Institute and Departments of Internal Medicine and Cellular and Molecular Physiology, Yale University School of Medicine, New Haven, Connecticut, USA. [4]Joslin Diabetes Center and Department of Medicine, Harvard Medical School, Boston, Massachusetts, USA. [5]Broad Institute of MIT and Harvard, Cambridge, Massachusetts, USA. [6]Center for Human Genetic Research, Massachusetts General Hospital, and Department of Systems Biology, Harvard Medical School, Boston, Massachusetts, USA. [7]Division of Endocrinology, Diabetes and Metabolism, Department of Medicine, Beth Israel Deaconess Medical Center and Harvard Medical School, Boston, Massachusetts, USA.

The transcriptional coactivator PPARγ coactivator 1α (PGC-1α) is a strong activator of mitochondrial biogenesis and oxidative metabolism. While expression of PGC-1α and many of its mitochondrial target genes are decreased in the skeletal muscle of patients with type 2 diabetes, no causal relationship between decreased PGC-1α expression and abnormal glucose metabolism has been established. To address this question, we generated skeletal muscle–specific PGC-1α knockout mice (MKOs), which developed significantly impaired glucose tolerance but showed normal peripheral insulin sensitivity. Surprisingly, MKOs had expanded pancreatic β cell mass, but markedly reduced plasma insulin levels, in both fed and fasted conditions. Muscle tissue from MKOs showed increased expression of several proinflammatory genes, and these mice also had elevated levels of the circulating IL-6. We further demonstrated that IL-6 treatment of isolated mouse islets suppressed glucose-stimulated insulin secretion. These data clearly illustrate a causal role for muscle PGC-1α in maintenance of glucose homeostasis and highlight an unexpected cytokine-mediated crosstalk between skeletal muscle and pancreatic islets.

Introduction

PPARγ coactivator 1α (PGC-1α) is a coactivator protein that binds to a number of transcription factors and augments their ability to induce target gene expression (1, 2). A central feature of PGC-1α is its potential to boost mitochondrial biogenesis and increase oxidative metabolism (3). In addition, PGC-1α regulates certain tissue-specific gene programs in vivo, such as increased myofibrillar gene expression associated with oxidative muscle fibers (4). PGC-1α is regulated in many tissues under a variety of physiological stimuli, including cold, exercise, and fasting (1, 2). In addition, dysregulation of PGC-1α mRNA expression has been observed in many disease states (1, 2). For example, PGC-1α expression is increased in the liver and islets of animal models of type 1 and type 2 diabetes (5, 6). In contrast, mRNA levels of PGC-1α, PGC-1β, and genes encoding for proteins involved in mitochondrial oxidative phosphorylation (OXPHOS) are reduced in skeletal muscle of human type 2 diabetics, at least in some populations (7, 8). The OXPHOS genes that are dysregulated in type 2 diabetic patients are under transcriptional control of PGC-1α, and signaling pathways by which PGC-1α controls OXPHOS gene expression in skeletal muscle have been elucidated (3, 7–13). Notably, PGC-1α dysregulation is also observed in pre-diabetic individuals, suggesting that reduction of PGC-1α levels is an early event in the development of the disease (7, 8).

Mitochondrial dysfunction has been closely associated with skeletal muscle insulin resistance in several studies (14–16). Decreased PGC-1α levels could theoretically trigger a pathway of pathology starting with reduced OXPHOS gene expression, decreased fatty acid oxidation, and subsequent lipid accumulation in skeletal muscle and culminating in insulin resistance and type 2 diabetes (8, 15, 16). However, the causality of PGC-1α dysregulation in skeletal muscle to the development of abnormalities in glucose homeostasis, particularly insulin resistance and type 2 diabetes, has never to our knowledge been directly tested in a loss-of-function model in vivo. Mice lacking PGC-1α in all tissues have been made, but these animals have many systemic abnormalities, including complete resistance to diet-induced obesity and hyperactivity secondary to central nervous system abnormalities (17, 18). This has made a serious examination of the role of skeletal muscle PGC-1α in systemic glucose homeostasis impossible in these animals (17, 18). These mice also have constitutively active AMP-activated protein kinase in skeletal muscle, which might compensate for the loss of PGC-1α in this tissue (17, 18). Therefore, to assess the importance of PGC-1α in peripheral tissues, tissue-specific knockout animals have to be generated. Proof of principle stems from liver-specific

Nonstandard abbreviations used: Cox, cytochrome *c* oxidase; GABP, GA-binding protein; MKO, skeletal muscle–specific PGC-1α knockout mouse; OXPHOS, oxidative phosphorylation; PGC-1α, PPARγ coactivator 1α; SDH, succinate dehydrogenase; SKM-Het, skeletal muscle–specific PGC-1α heterozygous mouse.

Conflict of interest: The authors have declared that no conflict of interest exists.

Citation for this article: *J. Clin. Invest.* **117**:3463–3474 (2007). doi:10.1172/JCI31785.

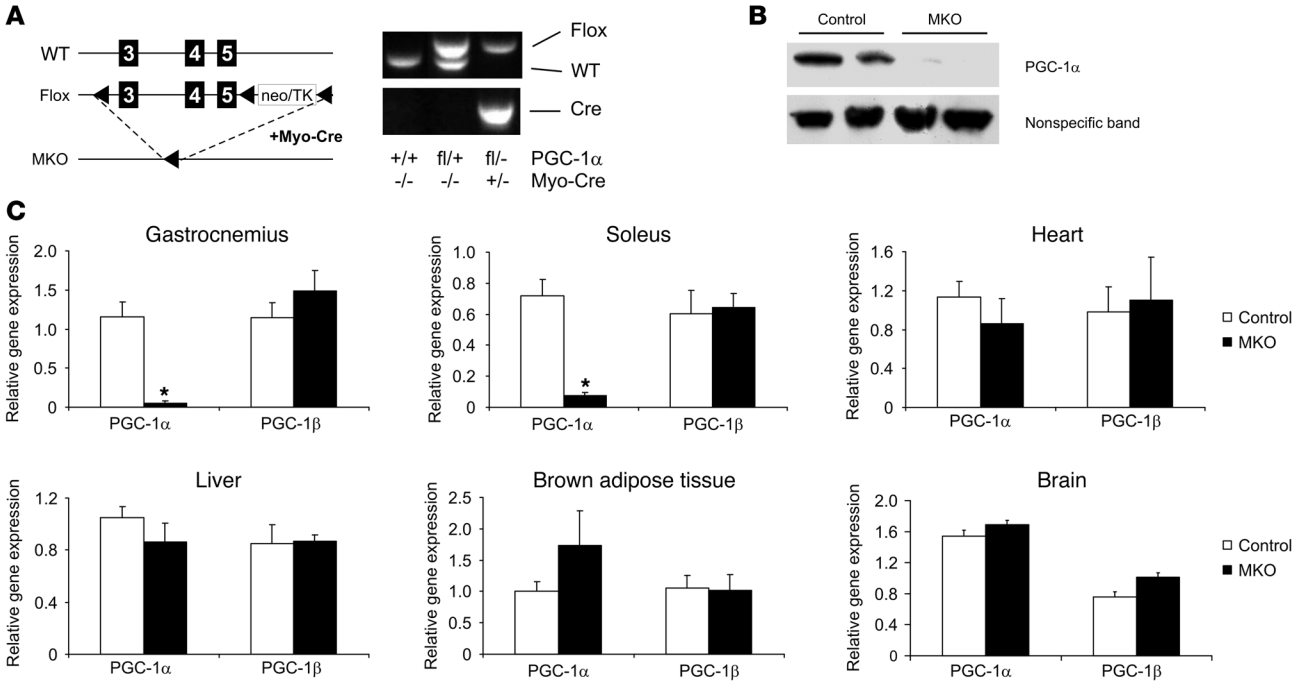

Figure 1
Generation and analysis of MKOs. (**A**) MKOs were generated by crossing mice with a floxed PGC-1α allele to animals that transgenically express cre recombinase under the control of the myogenin promoter and MEF2C enhancer (Myo-Cre). (**B**) PGC-1α protein levels in gastrocnemius muscle were determined by Western blot. (**C**) Relative PGC-1α and PGC-1β mRNA expression was measured in different tissues by real-time PCR. Values are mean ± SEM. *$P < 0.05$, MKO versus control. $n = 8$ per group.

PGC-1α knockout mice, which, in contrast to whole-body knockout mice, show the expected reduction of gene expression involved in gluconeogenesis and heme biosynthesis (19).

We thus generated skeletal muscle–specific PGC-1α knockout mice (MKOs) and studied the impact of aberrant PGC-1α levels in this tissue on glucose homeostasis and insulin sensitivity. Interestingly, while the loss of PGC-1α expression caused significant glucose intolerance, this intolerance was not associated with insulin resistance in peripheral tissues per se. Rather, we found an unexpected link between absence or reduction of PGC-1α expression in skeletal muscle and decreased insulin secretion in vivo. These data suggest an important crosstalk between skeletal muscle and pancreatic islets, perhaps via secretion of proinflammatory cytokines such as IL-6 by skeletal muscle.

Results

Generation and characterization of MKOs. MKOs were generated by breeding animals harboring a floxed PGC-1α allele (17) with mice that transgenically express cre recombinase under the control of the myogenin promoter and the MEF2C enhancer (20) (Figure 1A). The transcript and protein levels of PGC-1α were subsequently monitored by real-time PCR and Western blots, respectively. In gastrocnemius muscle, protein expression of PGC-1α was almost completely abolished (Figure 1B). Similarly, PGC-1α mRNA expression was drastically reduced in gastrocnemius and soleus muscles of MKOs (Figure 1C). Other known PGC-1α–expressing tissues such as heart, liver, brown adipose tissue, and brain were examined, and none of those had significantly altered PGC-1α transcript levels (Figure 1C). Thus, the ablation of PGC-1α in MKOs was restricted to skeletal muscle. Importantly, none of these tissues showed any compensatory adaptations in PGC-1β levels (Figure 1C). In terms of muscle function, MKOs has a lower expression of myosin heavy chains normally expressed in oxidative fibers (type I and IIa) and exhibits reduced voluntary physical activity (21).

Increase in mitochondrial function and oxidative metabolism are core functions of PGC-1α. We first studied the expression of metabolic genes and their corresponding transcription factors by real-time PCR. Two of the early PGC-1α target genes, estrogen-related receptor α (ERRα) and GA-binding protein A (GABPA), the DNA-binding subunit of GABP, showed reduced expression in MKOs compared with control mice (Figure 2A). These transcription factors are essential in controlling PGC-1α–induced OXPHOS expression in skeletal muscle (9, 10). Transcript levels of the more downstream transcription factors nuclear respiratory factor 1 and mitochondrial transcription factor A were unaltered in MKOs (Figure 2A). Nevertheless, expression of a number of OXPHOS and other mitochondrial genes was significantly reduced in MKOs, including the 1β subcomplex 5 and Fe-S protein 1 subunits of NADH-ubiquinone oxidoreductase, cytochrome *c*, cytochrome *c* oxidase (Cox) subunit 5b, and ATP synthase o subunit. These genes have been found to be directly regulated by ERRα, GABP, and PGC-1α (9, 10). Other OXPHOS genes did not differ in their expression between MKOs and controls, e.g., the NADH-ubiquinone oxidoreductase flavoprotein 2. Finally, non-OXPHOS mitochondrial genes that are known to be regulated by PGC-1α (19) were reduced in MKOs, for example the first enzyme in heme biosynthesis, 5-aminolevulinate synthase (Figure 2A). Notably, the reduction of mitochondrial gene expression observed in skeletal muscle of MKOs was equal to or even more dramatic than that previously reported in skeletal muscle of PGC-1α whole-body knockout ani-

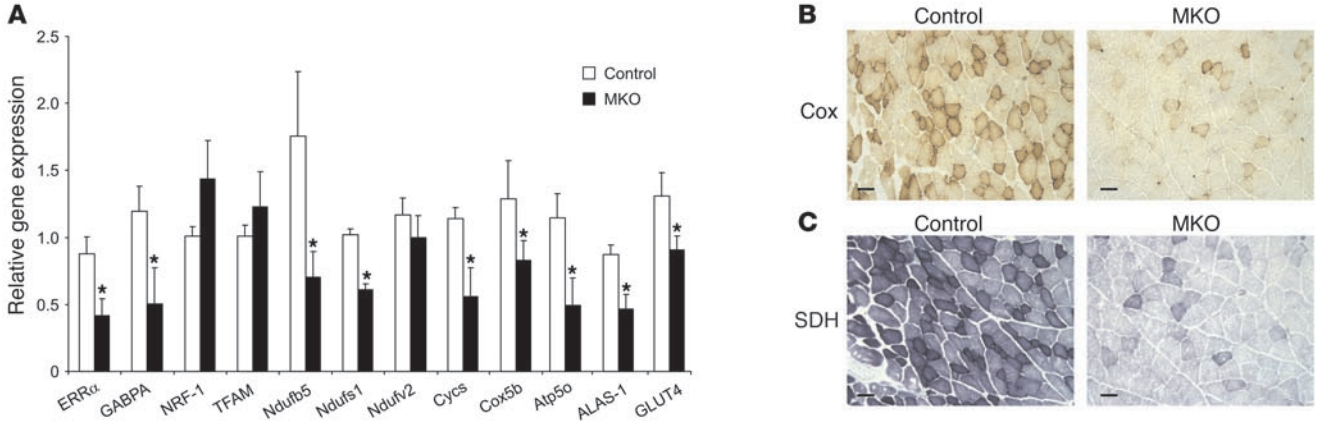

Figure 2

Decreased mitochondrial gene expression and function in MKOs. (**A**) RNA was isolated from gastrocnemius muscle, and relative gene expression was measured by semiquantitative real-time PCR and normalized to 18S rRNA levels. NRF-1, nuclear respiratory factor 1; TFAM, mitochondrial transcription factor A; Ndufb5, NADH-ubiquinone oxidoreductase 1β subcomplex 5; Ndufs1, NADH-ubiquinone oxidoreductase Fe-S protein 1; Ndufv2, NADH-ubiquinone oxidoreductase flavoprotein 2; Cycs, cytochrome *c*; Atp5o, ATP synthase o subunit; ALAS-1, 5-aminolevulinate synthase. (**B**) Cross-sections of gastrocnemius were stained for Cox activity. (**C**) Cross-sections of gastrocnemius were stained for SDH activity. Scale bars: 250 μM. Values are mean ± SEM. **P* < 0.05, MKO versus control. *n* = 8 per group.

mals (17). Finally, expression of the insulin-sensitive glucose transporter GLUT4 was likewise reduced in MKOs (Figure 2A). GLUT4 has previously been shown to be regulated by PGC-1α in skeletal muscle in gain of function in vitro and in vivo (4, 22).

Mitochondrial function was assessed by measuring the enzymatic activities of Cox and succinate dehydrogenase (SDH). Critical components of Cox are encoded by the mitochondrial genome, in contrast to SDH, which is encoded in the nucleus. Thus, Cox and SDH staining allows assessment of mitochondrial function in terms of the mitochondrial genome as well as nuclear encoded genes. Cox staining of gastrocnemius sections revealed a lower number of Cox-positive muscle fibers and a decreased intensity of Cox staining in MKOs (Figure 2B). SDH activity was likewise decreased in MKOs, and fewer fibers positive for SDH were found in gastrocnemius of MKOs (Figure 2C). Thus, skeletal muscle–specific ablation of PGC-1α reduced mitochondrial gene expression and mitochondrial function in terms of both nuclear- and mitochondrial-encoded genes. Morphologically, no differences in mitochondrial structure were detected (data not shown).

In many reported cases, reduced oxidative capacity correlates with decreased energy expenditure and increased body mass. Surprisingly, the body weight of PGC-1α MKOs fed either regular chow or a high-fat diet was less than that of their control littermates (Figure 3A). In terms of body composition, reduced fat mass and body fat percentage was seen in MKOs (Figure 3, B and C). A significant difference was observed around 10 weeks of age, both in mice fed high-fat diet (Figure 3D) and in mice fed regular chow diet (data not shown). Reduced body weight in MKOs was predominantly caused by a decreased rate of adipose tissue growth (Figure 3E). MKOs were hypophagic (Figure 3F) and exhibited an elevated basal metabolic rate, as suggested by increased heat production (Figure 3G) and elevated oxygen consumption (Figure 3H). In addition, CO_2 production was slightly, but significantly, elevated (Supplemental Figure 1A; supplemental material available online with this article; doi:10.1172/JCI31785DS1). The resulting decrease in the respiratory exchange ratio indicates a shift in substrate usage from glucose toward fat metabolism (Supplemental Figure 1B). In the blood, no significant difference in nonesterified fatty acids, total triglycerides, and glycerol was detected between control mice and MKOs (Supplemental Figure 1, C–E). Similarly, no difference in lipid accumulation in muscle tissue was detected by oil red O staining between control and MKO animals (data not shown). Decreased food intake and increased energy expenditure most likely explain the difference in body weight and fat mass between control and MKO mice. The higher basal metabolic rate in MKOs can potentially be explained by increased expression of the uncoupling protein 1 in brown adipose tissue, resulting in higher nonshivering thermogenesis (Supplemental Figure 2).

Abnormal glucose and insulin homeostasis in MKOs. To study the effect of PGC-1α dysregulation on glucose homeostasis, control animals and MKOs were fed either regular chow or a high-fat diet, and blood glucose was measured. MKOs fed regular chow had a significant elevation of blood glucose under fed conditions (Figure 4A) compared with controls. Glucose levels in MKOs and control mice were not different after an overnight fast (Figure 4A). This hyperglycemia in the MKOs was exacerbated by a high-fat diet, and glucose levels were higher in both fed and fasted MKOs, compared with their respective controls (Figure 4B). Blood glucose levels are controlled by the counter-regulatory hormones insulin and glucagon. Whereas no difference in glucagon levels was detected (data not shown), insulin was dramatically decreased in MKOs fed with regular chow or high-fat diet (Figure 4C). Depression of insulin levels in MKOs was likewise observed in fasted animals (data not shown).

Glucose intolerance in PGC-1α MKOs. The ability of control mice and MKOs to deal with an acute glucose load was assessed by glucose tolerance test. Both genotypes fed a regular chow diet had similar glucose excursion curves (Figure 4D). A trend toward glucose intolerance was found in MKOs, although only 2 data points reached a statistically significant difference. In contrast, MKOs fed a high-fat diet were clearly less able to deal with a glucose bolus, as indicated by the shift of the blood glucose curve (Figure 4E). Insulin tolerance tests were subsequently used to determine whether this glucose intolerance was associated with systemic insulin

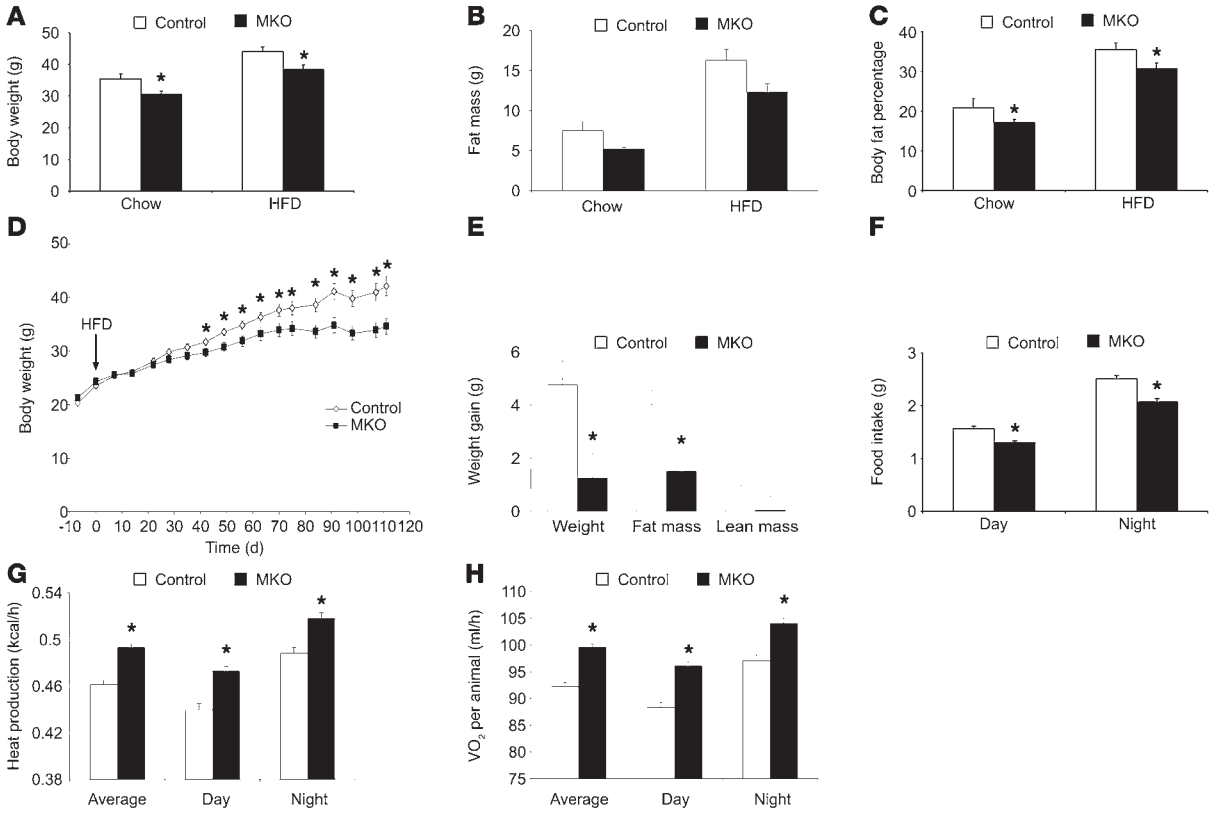

Figure 3
Decreased body fat and increased metabolic rate in MKOs. (**A**–**C**) Body weight (**A**), fat mass (**B**), and fat percentage (**C**) in 10-week-old mice fed regular chow or high-fat diet (HFD). (**D**) Growth curve of control mice and MKOs on a high-fat diet. (**E**) Weight gain (total, lean mass, and fat mass) in control and MKO animals fed a high-fat diet for 3 weeks. (**F**–**H**) Food intake (**F**), heat production (**G**), and oxygen consumption (VO_2) per animal (**H**) were determined using a comprehensive laboratory animal monitoring system with control animals and MKOs on a high-fat diet. *$P < 0.05$, MKO versus control. $n = 6$ per group.

resistance. In fact, the capacities of control animals and MKOs to regulate blood glucose levels after a bolus of insulin were indistinguishable (Figure 4F). Similarly, no difference in the blood glucose curves in insulin tolerance tests performed with regular chow–fed animals was found (data not shown).

To further investigate the glucose intolerance with apparently normal insulin sensitivity in the MKOs, we measured blood insulin and glucose simultaneously in a glucose tolerance test. Interestingly, in addition to the lower basal insulin, insulin levels following glucose administration were lower in MKOs than in control mice (Figure 4G). In parallel, blood glucose levels in MKOs exceeded those found in control mice (Figure 4H). Thus, MKO animals have aberrant glucose homeostasis that manifests in hyperglycemia under different conditions. This elevation of blood glucose seems more likely to be caused by the observed hypoinsulinemia than a systemic insulin resistance.

Increased peripheral insulin–dependent glucose uptake in MKOs. We tested this hypothesis by performing hyperinsulinemic, euglycemic clamps, which allow very accurate determination of insulin-dependent glucose uptake in vivo. First we tested whether the hyperglycemia could be the result of elevated gluconeogenesis in the liver. Hepatic glucose output was measured under basal and clamped conditions; no difference was detected between MKOs and controls in either condition (Figure 5A). A second possible explanation for the hyperglycemia is decreased insulin-dependent glucose uptake into skeletal muscle and fat. Surprisingly, MKOs were found to take up significantly *more* glucose and channel this glucose into glycolysis under hyperinsulinemic conditions (Figure 5B). Thus, as opposed to the hypothesis that PGC-1α dysregulation causes insulin resistance, MKOs in fact have increased peripheral insulin sensitivity. In parallel, the insulin signaling pathways in skeletal muscle and liver were analyzed; in agreement with the data obtained from the hyperinsulinemic, euglycemic clamps, an increase in Akt activity in skeletal muscle was found while IRS-1–PI3K activity remained unchanged (Supplemental Figure 3A). In contrast, neither Akt nor IRS-2–PI3K activities were altered in the livers of MKOs compared with control mice (Supplemental Figure 3B), underlining the findings that hepatic insulin sensitivity is not affected by muscle-specific PGC-1α ablation.

Abnormal pancreatic islet morphology in MKOs. The combination of the striking hypoinsulinemia and hyperglycemia and the data showing normal hepatic glucose output and even increased peripheral glucose disposal under hyperinsulinemic conditions suggested that the pancreatic β cells might be the culprits for the abnormal glucose homeostasis in MKOs. Morphological analysis revealed grossly enlarged islets in MKOs compared with controls (Figure 6A). Morphometric analyses confirmed larger islet size in MKOs quantitatively (Figure 6B). Moreover, these studies showed that the

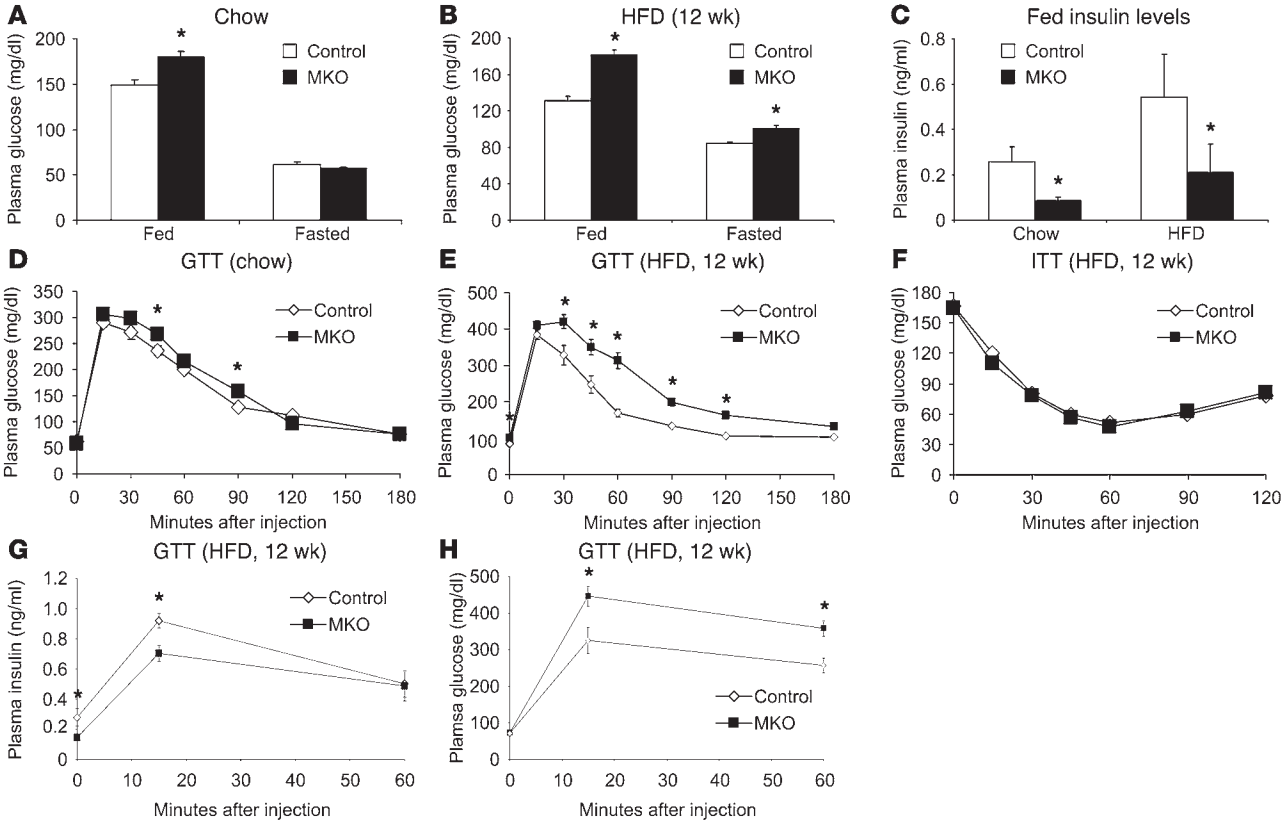

Figure 4

Impaired glucose homeostasis in MKOs. (**A**) Blood glucose was determined in fed and fasted mice (16 h, overnight) that were fed regular chow diet. (**B**) Blood glucose was determined in fed and fasted mice (16 h, overnight) that were fed a high-fat diet for 12 weeks. (**C**) Blood insulin was determined in nonfasted mice that were fed a high-fat diet for 12 weeks. (**D** and **E**) Glucose tolerance test (GTT) in regular chow–fed (**D**) and high-fat diet–fed (**E**) mice. Mice were given a bolus i.p. injection of 2 g/kg glucose, and blood glucose was subsequently measured at the indicated time points. (**F**) Insulin tolerance test (ITT) in high-fat diet–fed mice. Mice were given a bolus i.p. injection of 0.8 U/kg insulin, and blood glucose was subsequently measured at the indicated time points. (**G** and **H**) Glucose tolerance test in high-fat diet–fed mice. Mice were given a bolus i.p. injection of 2 g/kg glucose. Blood insulin (**G**) and glucose (**H**) were simultaneously measured at the indicated time points. *$P < 0.05$, MKO versus control. $n = 8$ per group.

individual β cells in MKO islets were smaller than those found in islets from control animals (Figure 6, C and D). The smaller size of β cells and the larger area covered by MKO islets imply a higher number of pancreatic β cells in MKOs. Importantly, we did not observe any significant differences in the size or number of pancreatic α and δ cells in MKO islets compared with that in control islets (Figure 6B and data not shown). In addition, the overall architecture of the islets appeared normal. Finally, no sign of increased β cell apoptosis was detected (data not shown). To rule out unexpected recombination of the PGC-1α gene in islets of the MKO mice, we examined isolated islets for expression of PGC-1α, PGC-1β, and several PGC-1α target genes. Furthermore, we measured cre expression in isolated islets and genotyped islet genomic DNA for recombination events in the PGC-1α allele. None of these data indicated *any* gene deletion or change in expression of PGC-1α in islets (Supplemental Figure 4). Furthermore, no alterations in mitochondrial gene expression in isolated MKO islets compared with control islets were found (Supplemental Figure 4).

Islets were subsequently isolated from control mice and MKOs and cultured for 2 days; these islets were tested for their ability to perform glucose-stimulated insulin secretion. First, we found no difference in total insulin content between control and MKO islets when normalized to DNA content (Figure 6E) Second, insulin secretion in low- and high-glucose conditions was comparable between islets from control animals and MKOs (Figure 6F). Together, these data suggest that insulin secretion in isolated, cultured islets in MKOs is normal and is consistent with the idea that an extrinsic factor, presumably arising directly or indirectly from muscle of the MKOs, is having a negative action on islets in vivo.

MKOs have increased expression of several proinflammatory cytokines and circulating IL-6 concentration. Factors released by white adipose tissue, adipokines, are well known to alter systemic glucose homeostasis, insulin sensitivity, and insulin secretion (23–25). Much less is known about factors produced and secreted by skeletal muscle in this context. Recently, certain proinflammatory cytokines, myokines, have been recognized as circulating factors that are able to modulate glucose and insulin homeostasis (26). Moreover, low-grade inflammation is observed in skeletal muscle tissue of obese and type 2 diabetic patients (27). We thus measured the expression of a broad range of genes encoding proteins involved in inflammation in skeletal muscle. Interestingly, several of these genes were elevated in skeletal muscle of MKOs com-

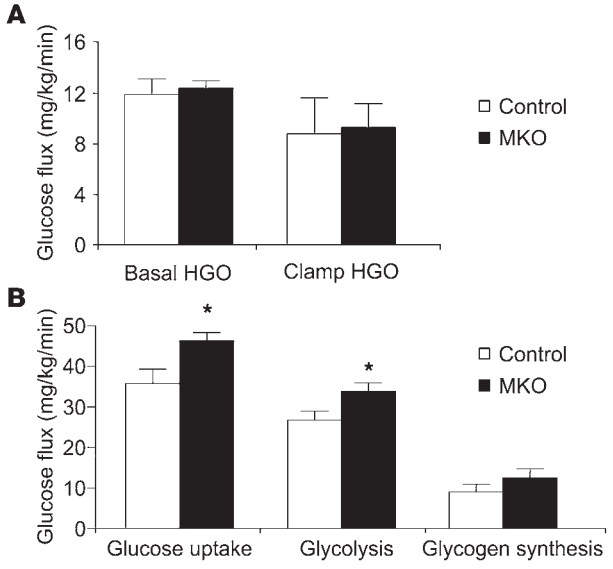

Figure 5
Systemic glucose fluxes and insulin sensitivity. (**A**) Hyperinsulinemic, euglycemic clamps were used to measure hepatic glucose output (HGO) under basal and clamped conditions. (**B**) Systemic glucose uptake, glycolysis, and glycogen synthesis were determined in hyperinsulinemic, euglycemic clamps. Values are mean ± SEM. *$P < 0.05$, MKO versus control. $n = 7$ (controls); 10 (MKOs).

pared with control mice, including SOCS1, SOCS3, TNF-α, IL-6, and CD68 (Figure 7A). Moreover, a marked elevation of serum IL-6 was found in MKOs (Figure 7B). The elevation in MKOs was similar to the increase of circulating IL-6 in mouse models with high-fat diet–induced obesity (28). In contrast, TNF-α serum levels were similar in control mice and MKOs (data not shown). It is unclear at present whether the observed increase in inflammatory genes and circulating cytokines is mediated by muscle fibers or by immune cell infiltration. However, we observed regulation of IL-6, TNF-α, and SOCS3 in a PGC-1α–dependent manner in isolated muscle cells in culture, on both the mRNA and the protein level (Supplemental Figure 5), which suggests that skeletal muscle contributes to the systemic release of cytokines in MKOs. Accordingly, we could not find any indication of increased infiltration of MKO muscle tissue by mononuclear cells (Supplemental Figure 5D).

The effect of IL-6 on insulin secretion was tested in islets isolated from control and MKO mice. First, 24 h of IL-6 treatment reduced glucose-stimulated insulin secretion under high-glucose conditions in islets from both control mice and MKOs (Figure 7, C and D). Interestingly, neither amino acid–mediated (10 mM L-arginine) nor glucagon-like peptide–1–mediated (100 nM) changes in insulin secretion were significantly altered by IL-6. Importantly, no significant differences in the extent of insulin secretion under any of the conditions tested was observed between islets isolated from control mice and MKOs (Figure 7, C and D). These findings indicate that IL-6 only inhibits glucose-stimulated insulin secretion, and does not extend to other secretagogues. Thus, the IL-6–mediated inhibition of insulin secretion implies specific regulation of this pathway, instead of general inflammation being the mediator of the observed effect. In fact, no increase in inflammation or apoptosis was found in the pancreata of MKOs (data not shown). Moreover, the absence of significant differences in insulin secretion in isolated islets in vitro is consistent with the notion that circulating factors, presumably secreted from skeletal muscle, are responsible for the alterations in insulin levels in MKOs in vivo.

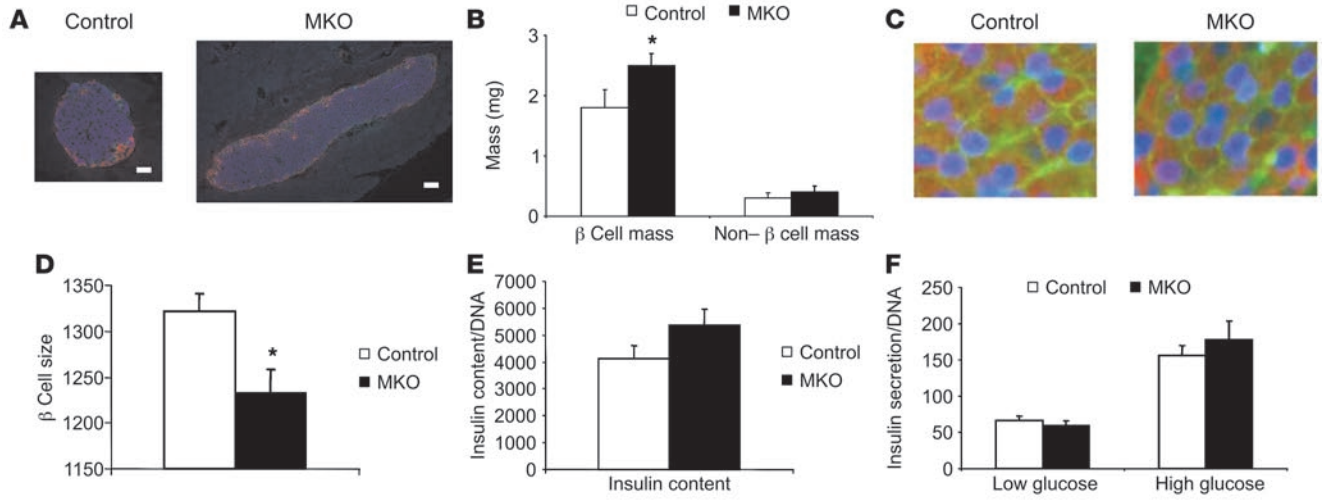

Figure 6
Islet morphology, insulin content, and glucose-stimulated insulin secretion. (**A**) Fixed pancreatic sections were immunostained for insulin (blue), glucagon (red), and somatostatin (green). Islets pictured are representative of control mice and MKOs shown at the same scale (original magnification, ×40). Scale bars: 50 μM. (**B**) Quantitative analysis of β cell and non–β cell mass. Mass was measured by quantifying islets sections stained with markers for the different islet cell types. (**C**) β-Catenin staining of islet sections. Islet sections were stained with antibodies against insulin (red) and β-catenin (green) as well as DAPI (blue) to visualize nuclei. Original magnification, ×100. (**D**) Quantification of β cell size. The cellular area outlined by cell membrane stained for β-catenin was measured as the size of individual cells. (**E**) Insulin content of isolated islets was determined and normalized to the amount of DNA. (**F**) Insulin secretion normalized to the amount of DNA from isolated islets was determined under low-glucose (3.3 mM) and high-glucose (16.7 mM) conditions. Values are mean ± SEM. *$P < 0.05$, MKO versus control.

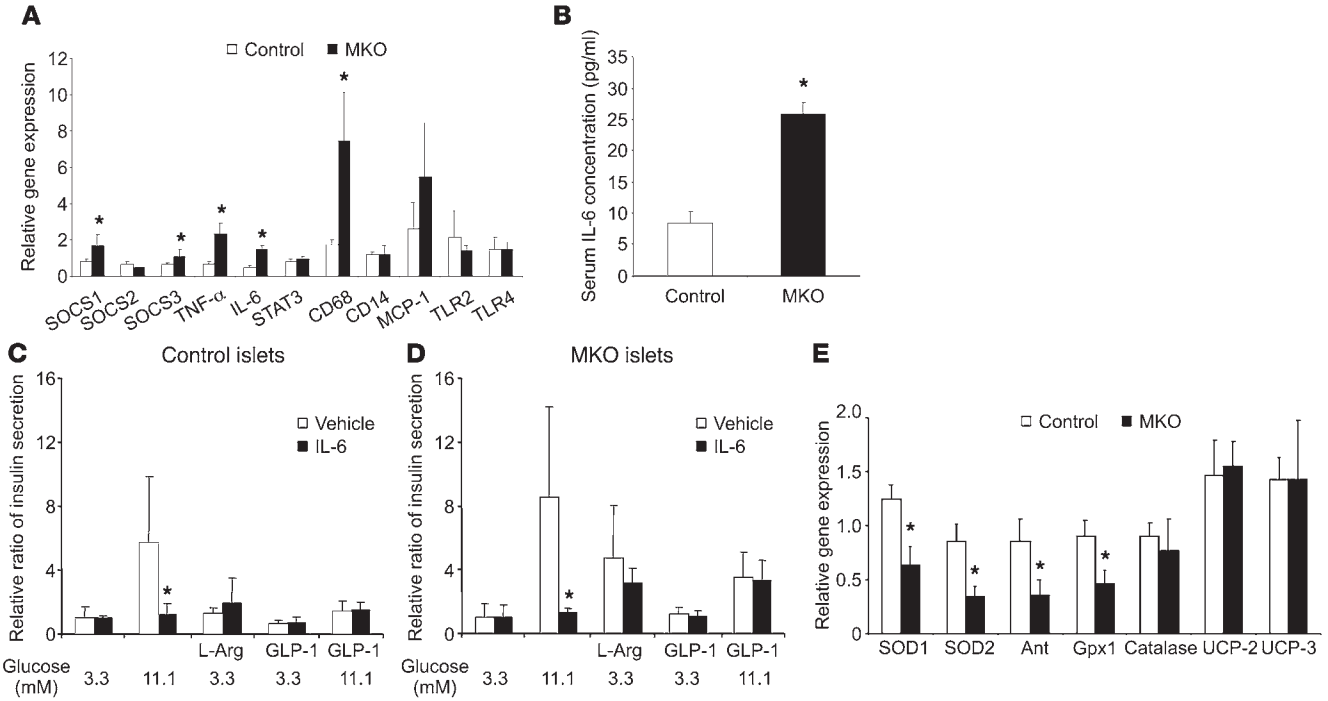

Figure 7

Elevated markers for inflammation and ROS in MKOs. (**A**) Expression of several genes associated with inflammation in skeletal muscle were determined in gastrocnemius of control and MKO mice. MCP-1, monocyte chemotactic protein–1. (**B**) Serum IL-6 concentration was determined in control and MKO mice. (**C** and **D**) IL-6 inhibited glucose-stimulated insulin secretion in isolated islets from control mice (**C**) and MKOs (**D**). Isolated islets from control mice and MKOs were incubated for 24 h in RPMI media supplemented with 7 mM glucose and 10% FCS, followed by another 24-h incubation with vehicle or 400 pg/ml IL-6. At 48 h after isolation, static incubation experiments were performed. Stimulated insulin secretion was standardized by basal insulin secretion during preincubation period from same islet samples, and relative secreted insulin was normalized to the insulin secretion under 3.3 mM glucose. The glucose concentration used for stimulation is indicated. L-Arg, L-arginine (10 mM); GLP-1, glucagon-like peptide–1 (100 nM). Values are mean ± SD from 3–5 individual batches of islets. (**E**) ROS-detoxifying gene expression was analyzed in gastrocnemius of control mice and MKOs. SOD, superoxide dismutase; Ant, adenine nucleotide translocator; Gpx, glutathione peroxidase; UCP, uncoupling protein. Values are mean ± SEM. $^*P < 0.05$, MKO versus control. $n = 8$ per group.

Production of IL-6 mRNA in skeletal muscle can be stimulated by ROS (29). PGC-1α is critically involved in the regulation of ROS-detoxifying genes in different tissues, and lack of PGC-1α results in elevated levels of ROS (30). In accordance with previous results from studies of ROS-detoxifying gene expression in the brains of PGC-1α whole-body knockout animals (30), we found that expression of several of these detoxifying genes was reduced in skeletal muscle of MKOs compared with control mice (Figure 7E). Interestingly, transcript levels for both mitochondrial and cytoplasmic ROS-detoxifying genes were reduced, underlining the importance of PGC-1α in this pathway. The decreased expression of these genes and the expected increase in ROS in skeletal muscle are possible reasons for the elevated transcription of IL-6 in MKOs.

Abnormal glucose homeostasis in skeletal muscle–specific PGC-1α heterozygous animals. Humans with type 2 diabetes have a quantitative reduction but not an elimination of PGC-1α expression. To examine the effects of a partial reduction in PGC-1α expression, we also analyzed skeletal muscle–specific PGC-1α heterozygous mice (SKM-Hets). These animals showed about 50% reduction in PGC-1α mRNA and protein levels in skeletal muscle and had no change in PGC-1α or PGC-1β expression in other tissues (Supplemental Figure 6). Accordingly, expression of mitochondrial genes in SKM-Hets was more modestly reduced than that in MKOs, around 15%–20% (data not shown). In terms of their glucose homeostasis, SKM-Hets recapitulated the metabolic key findings of the MKOs. Like MKOs, SKM-Hets fed either regular chow or high-fat diet were both more glucose intolerant than control animals (Figure 8, A and B).

Systemic insulin sensitivity, as ascertained in insulin tolerance tests, was unchanged in SKM-Hets fed either regular chow or high-fat diet (Figure 8, C and D). Similarly, glucose uptake into peripheral tissues of SKM-Hets was not significantly different from the uptake in control animals in hyperinsulinemic, euglycemic clamps (data not shown). Although SKM-Hets did not show an overt hypoinsulinemia like MKOs, insulin release was significantly delayed upon a bolus injection of glucose in vivo (Figure 8, E and F). Moreover, IL-6 mRNA expression and IL-6 serum concentrations were increased in SKM-Hets compared with control animals (Figure 8, G and H). Finally, the expression of several ROS-detoxifying genes was reduced in SKM-Hets (Supplemental Figure 7). Thus, even a 50% reduction in skeletal muscle PGC-1α expression triggered this organ crosstalk and altered insulin secretion from pancreatic β cells. Importantly, this decrease of PGC-1α transcript levels in SKM-Hets was equivalent to the PGC-1α mRNA dysregulation observed in type 2 diabetic patients and individuals with an increased risk of developing diabetes due to their family history (8). Importantly, these findings were selective for skeletal muscle–specific heterozygosity of PGC-1α and were not observed in whole-body PGC-1α heterozygous animals, which were used as controls here; the tissue-

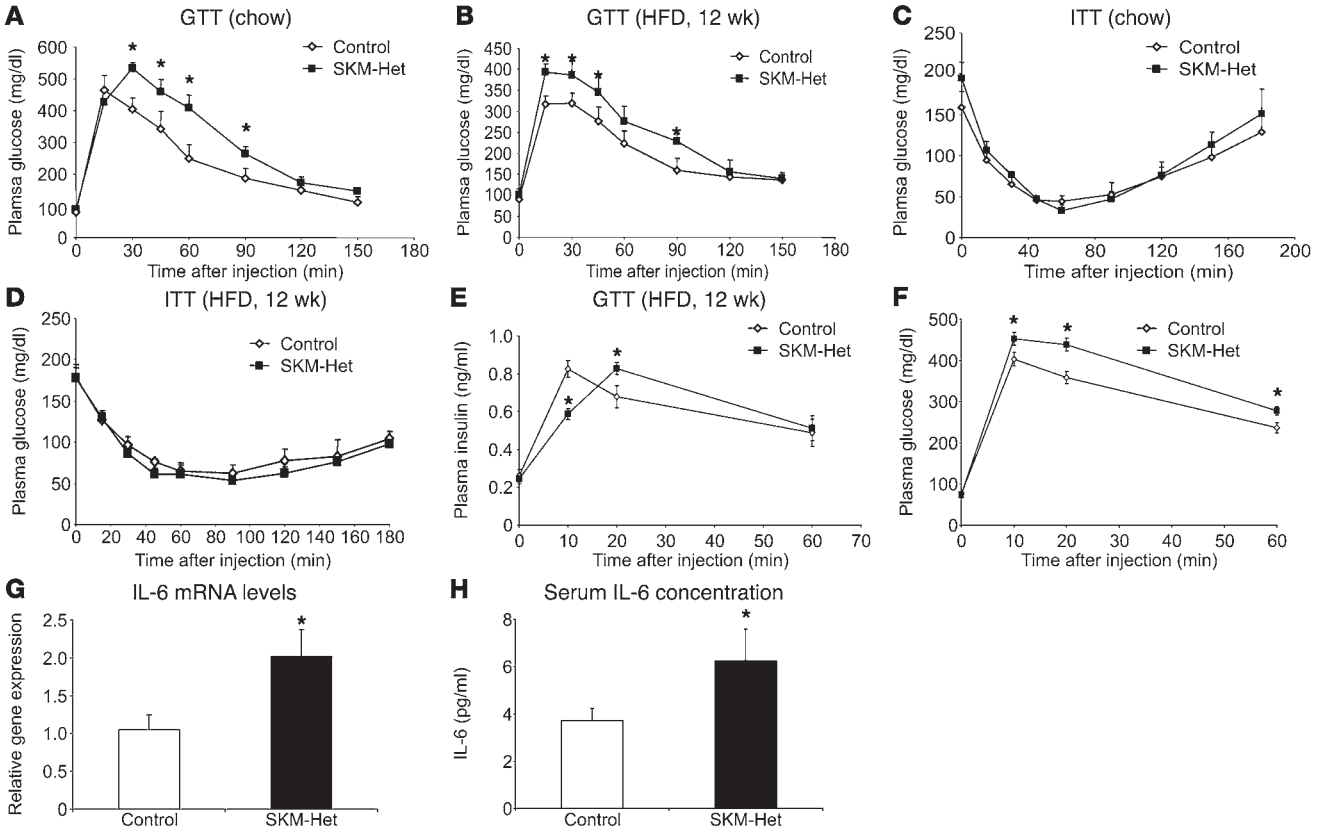

Figure 8

Glucose and insulin homeostasis in SKM-Hets. (**A** and **B**) Glucose tolerance tests in control mice and SKM-Hets fed regular chow (**A**) or high-fat diet (**B**). (**C** and **D**) Insulin tolerance tests in control mice and SKM-Hets fed regular chow (**C**) or high-fat diet (**D**). (**E** and **F**) Glucose tolerance tests in control mice and SKM-Hets fed a high-fat diet with simultaneous determination of blood insulin (**E**) and blood glucose (**F**). (**G** and **H**) Determination of IL-6 mRNA levels in gastrocnemius (**G**) and serum IL-6 concentration (**H**) in control and SKM-Het mice. Values are mean ± SEM. **P* < 0.05, SKM-Het versus control. *n* = 8 per group.

specific knockouts exhibited clear differences from the whole-body PGC-1α heterozygous mice (Supplemental Figure 8).

Correlation between IL-6 and PGC-1α gene expression in skeletal muscle of human type 2 diabetics. Our findings in mouse models suggest an important regulatory role for PGC-1α in controlling expression of IL-6 and other proinflammatory molecules in skeletal muscle. The significance for humans of these results in rodents was tested by further analysis of gene expression data from a set of 42 diabetic and glucose-intolerant individuals who were subjected to muscle biopsies previously (7). In this population, we found a highly significant correlation between mRNA expression of IL-6 and the PGC-1α gene (*PPARGC1A*) in skeletal muscle (Figure 9A). Interestingly, other clinical parameters, including body mass index (BMI), did not correlate with IL-6 gene expression (Figure 9B). Expression of another inflammatory cytokine produced by skeletal muscle, TNF-α, also correlated with PGC-1α transcript levels (Figure 9C). Again, BMI did not correlate with TNF-α levels (Figure 9D). Thus, relative PGC-1α mRNA expression was a strong predictor of gene expression of IL-6 and other inflammatory cytokines in skeletal muscle, independent of other clinical variables assayed in these human subjects.

Discussion

PGC-1α is a key regulator of mitochondrial function and oxidative metabolism in skeletal muscle. The loss of PGC-1α shown here via tissue-specific ablation showed definitively that PGC-1α was necessary for normal regulation of mitochondrial gene expression in this tissue. Reduced PGC-1α and OXPHOS levels have been associated with insulin resistance and type 2 diabetes in humans (7, 8) and mice (31). We therefore focused our attention on glucose and insulin homeostasis in MKOs and SKM-Hets. Our data show clearly that a reduction of PGC-1α levels in skeletal muscle, and the subsequent reductions in OXPHOS gene expression, were not causally linked to systemic insulin resistance, at least under the conditions studied here. Of course, it cannot be ruled out that decreases of PGC-1α and OXPHOS genes might contribute to insulin resistance in muscle under other experimental conditions, such as in aging or during prolonged periods of hyperglycemia. The data about insulin sensitivity in MKOs are surprising in light of the reduced expression of GLUT4 and various mitochondrial genes in skeletal muscle of the MKOs, suggesting that unidentified compensatory systems might be operating in these mice. These data are also consistent with results observed in mice containing a mutation in PGC-1β. These animals have reduced mitochondrial gene expression in the absence of hyperactivity, but show no evidence of insulin resistance in skeletal muscle (32). It is possible that the reduced body fat mass increases insulin sensitivity in MKOs above that of control mice. In contrast, SKM-Hets exhibited body fat mass and insulin sensitivity that was not significantly different from that observed in control

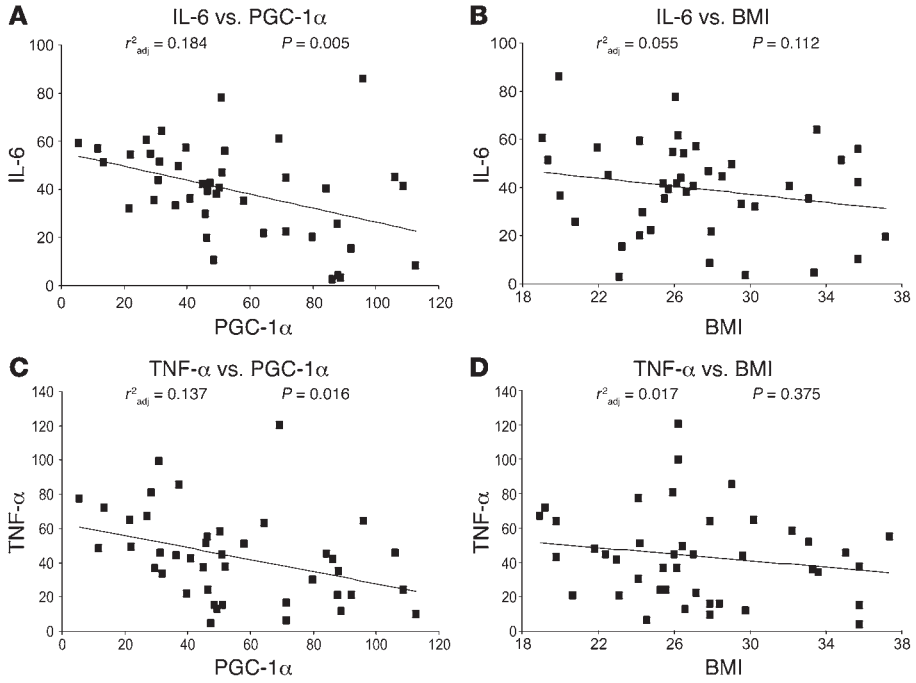

Figure 9
Correlation between PGC-1α and IL-6 gene expression in skeletal muscle of humans. (**A**–**D**) Linear regression analysis of IL-6 and PGC-1α (*PPARGC1A*) gene expression (**A**), IL-6 gene expression and BMI (**B**), TNF-α and PGC-1α gene expression (**C**), and TNF-α gene expression and BMI (**D**) in skeletal muscle of 42 human volunteers. Adjusted r^2 (r^2_{adj}) and *P* values are shown.

animals (Supplemental Figure 9 and data not shown). Body weight, fat mass, fat percentage, growth curves, and food intake were not significantly altered in SKM-Hets (Supplemental Figure 9, A–E). Accordingly, basal energy expenditure in SKM-Hets was not significantly different than that of control animals (Supplemental Figure 9, F and G). Finally, no shift in substrate usage or alteration in blood lipid levels was detected in SKM-Hets (Supplemental Figure 10).

Importantly, glucose homeostasis is disturbed with loss of one or both alleles of PGC-1α in skeletal muscle, and the homozygous mutants are severely hypoinsulinemic. Muscle-specific heterozygotes showed a delay in insulin release during a glucose tolerance test, possible because of impaired first-phase insulin secretion. This might contribute to the impaired glucose tolerance observed in these animals. Thus, a reduction of PGC-1α expression results in a surprising crosstalk between muscle and pancreatic β cells. In theory, this crosstalk could be mediated by a variety of molecules, including circulating lipids or peptides, or could even involve CNS signals to the islets. However, the most obvious candidates here are the cytokines. IL-6 is one of the best-studied circulating factors that is produced by skeletal muscle and other metabolic tissues and has a wide range of effects on insulin sensitivity and insulin secretion (33). In fact, IL-6 has been introduced as the first myokine, a cytokine that is produced and secreted by contracting muscle fibers and exerts effects on other organs (26). Although IL-6 has been proposed to mediate antiinflammatory effects of exercise, aberrant IL-6 levels have been shown to be proinflammatory in other contexts, and its exact role remains controversial (33). Importantly, IL-6 has been shown to inhibit glucose-stimulated insulin secretion in isolated murine islets without being cytotoxic (34, 35). In contrast, an acute increase in IL-6 levels has no significant effect on serum insulin concentration in either rodents or humans in vivo (33). In fact, similar to our findings in the MKOs, short-term infusion of IL-6 does not induce insulin resistance in rats in vivo despite SOCS3 induction (36). Moreover, IL-6 knockout animals have normal insulin levels, although they develop obesity at the age of 6–7 months (33). To our knowledge, no experimental study with chronically and specifically elevated IL-6 exists to date.

Elevation of other cytokines produced and released by skeletal muscle has been implicated in altering systemic insulin sensitivity and insulin release; these cytokines include TNF-α, IL-1β, and IL-15 (37–40). Thus, while IL-6 represents a convenient marker to show elevated circulating cytokine levels in MKOs, it is likely that other secreted factors also contribute to the observed phenotype. In fact, several markers for inflammation are elevated in skeletal muscle of MKOs (Figure 7A). Moreover, recent experiments have shown that there is extensive crosstalk between different cytokines in type 2 diabetes, for example, between IL-1 and IL-6 (41). A more global study of the levels of secreted factors in the blood of MKOs may untangle this web in the future. Nevertheless, in the present study we showed evidence of an inhibitory action of IL-6 on glucose-stimulated insulin secretion in isolated islets (Figure 7, C and D). Moreover, a contribution of IL-6 to the islet dysfunction was implied by elevated SOCS3 and endogenous IL-6 mRNA levels in the pancreata of MKOs (Supplemental Figure 11).

A likely explanation for the elevation of several proinflammatory genes in the muscle of MKOs is the stimulatory effect of increased ROS levels secondary to reduced expression of ROS-detoxifying genes in MKOs. In skeletal muscle, IL-6 transcription is stimulated by NF-κB, which in turn can be activated by ROS or calcium signaling in this tissue (42). Alternatively, increased oxidative stress, low glucose availability, and low glycogen content are capable of inducing heat shock proteins that in turn, via heat shock factors 1 and 2, activate IL-6 synthesis in muscle (42). The ability of PGC-1α to suppress ROS has been observed in multiple tissues (30, 43, 44). It is also conceivable that PGC-1α itself could have more direct antiinflammatory effects in skeletal muscle, because it has previously been shown that the closely related PGC-1β attenuates macrophage-mediated inflammation (45).

The organ crosstalk shown here suggests a potentially important and novel mechanism contributing to the failure of pancreatic β

cells to adequately secrete insulin in human type 2 diabetes. Most current models of β cell desensitization and exhaustion imply that hypoinsulinemia is a late event in type 2 diabetes caused by glucotoxicity and β cell apoptosis (46). However, β cell function and mass decrease progressively, sometimes at very early stages of the disease (47). Thus, reduction of PGC-1α levels in skeletal muscle of some predisposed human populations might contribute to a decrease in insulin secretion through the actions of myokines such as IL-6 and others without causing β cell apoptosis. In fact, our analysis showed that IL-6 and TNF-α mRNA levels in human skeletal muscle was strongly and negatively associated with PGC-1α gene expression. Strikingly, BMI, fasting glucose and fasting insulin levels did not correlate with IL-6 and TNF-α levels (Figure 8 and Supplemental Table 1). Once insulin resistance is promoted by factors other than PGC-1α dysregulation, β cell desensitization and apoptosis might be stimulated by other factors, although even here, myokines regulated by PGC-1α might contribute to impaired function. It will be important to study the implication of skeletal muscle–specific dysregulation of PGC-1α on amino acid–induced insulin secretion in the future. PGC-1α is thought to affect protein biosynthesis and degradation rates in skeletal muscle (9, 48) and thereby could potentially alter the levels of amino acids that change pancreatic insulin secretion. Experiments in isolated islets in vitro showed no inhibitory effect of IL-6 on L-arginine–mediated changes in insulin secretion (Figure 7, C and D). In summary, our findings highlight the importance of skeletal muscle PGC-1α as a regulator of the myokine expression and suggest further studies of muscle-islet crosstalk in diabetes. In addition, these results also suggest a plausible mechanism for how muscle, particularly in the context of metabolic disease and/or exercise, might talk to other organ and tissue systems, including blood vessels, heart, and brain.

Methods

MKOs and heterozygous mice. The generation of mice with a floxed PGC-1α allele has been described previously (17). To obtain muscle-specific knockout animals, mice with a floxed PGC-1α allele were crossed with animals transgenically expressing cre recombinase under the control of the myogenin promoter and MEF2C enhancer (a generous gift from R. Bassel-Duby and E.N. Olson, University of Texas Southwestern, Dallas, Texas, USA) (20). However, male mice with the floxed PGC-1α allele are infertile because of the presence of the neomycin cassette. Thus, muscle-specific knockout animals could only be obtained in mice with 1 floxed and 1 knockout allele of PGC-1α (lox/–, myogenin-cre). As control mice, we used a mixed population of different mice heterozygous for PGC-1α (lox/–; +/–; and +/–, myogenin-cre). The different genotypes used as controls were tested for blood glucose and IL-6 levels, and no differences were found (Supplemental Figure 12, A and B). Moreover, no difference in PGC-1α expression levels between wild-type and lox/+ mice was detected in muscle, heart, brown adipose tissue, liver, and brain (Supplemental Figure 13). Specifically, the breeding strategy was to cross –/–, myogenin-cre males with lox/+ females. Thus, offspring was of the following genotypes: lox/–; +/–; lox/–, myogenin-cre; and +/–, myogenin-cre. All these genotypes were found in Mendelian ratio at the age of 21 days (Supplemental Table 2). SKM-Hets had 1 floxed and 1 wild-type PGC-1α allele together with cre expression under the control of the myogenin promoter (lox/+, myogenin-cre). For this group, we also used a mixed population of animals as controls (+/+; +/+, myogenin-cre; and lox/+). No difference in blood glucose and IL-6 levels were observed in control animals with these different genotypes (Supplemental Figure 12, C and D). In this case, the breeding was achieved by crossing +/+, myogenin-cre males with lox/+ females. Accordingly, pups were of the following genotypes: +/+; lox/+; +/+, myogenin-cre; and lox/+, myogenin-cre. Again, pups of the different genotypes were found in Mendelian ratio at the age of 21 days (see Supplemental Table 3). Since the mice have a mixed C57BL/6 and 129 background, littermates were used in all experiments. Groups of 8 male mice were used in all experiments unless stated otherwise. Genotyping and analysis of genomic DNA in isolated islets was performed using primers that detect the wild-type allele, the knockout allele, one of the loxP sites, and cre recombinase. Animals were fed a regular chow diet or a high-fat diet (58% kcal from fat; Research Diets Inc.). All experiments and protocols were approved by the Institutional Animal Care and Use Committees of the Dana-Farber Cancer Institute, the Beth Israel Deaconess Medical Center, Yale University, and the Joslin Diabetes Center.

Culture and treatment of C2C12 and primary muscle cells. C2C12 and primary mouse muscle cells were isolated and cultured as described previously (49). C2C12 cells were differentiated into myotubes and infected with adenoviral-encoded GFP and PGC-1α. After 48 h, cells were harvested and used for analysis. Primary muscle cells of control and global PGC-1α knockout animals were differentiated into myotubes, and mRNA and secreted IL-6 protein levels were measured after 6 days.

Protein isolation and Western blot. Muscle tissue was homogenized in RIPA buffer and 150 μg of proteins separated by SDS-PAGE. PGC-1α protein was detected using a custom antibody generated against the N terminus of PGC-1α (50).

RNA isolation and quantification. TRIzol reagent (Invitrogen) was used to isolate total RNA from different tissues according to the manufacturer's instructions. After a DNase digest, 1 μg of total RNA was reversed transcribed. The resulting cDNA was subsequently analyzed on an Applied Biosystems Real-Time PCR System 7300 using the ΔδCt threshold cycle method. Relative gene expression was normalized to 18S rRNA levels.

Dual energy X-ray absorptiometry scan. Body fat content was determined by dual energy X-ray absorptiometry on anesthetized mice (Piximus II; Lunar Corp.).

Comprehensive laboratory animal monitoring system. Comprehensive laboratory animal monitoring system (CLAMS; Columbia Instruments) analysis was performed for 4 light and 3 dark periods after an acclimatization of 2 days. Data about oxygen consumption, CO_2 production, respiratory exchange ratio, heat, and food intake were collected every 48 minutes on 16 mice simultaneously.

Analysis of blood lipids. Serum nonesterified fatty acids were determined using the NEFA Determination Kit (Wako Chemicals). Serum triglycerides and glycerol were measured with the Serum Triglyceride Determination Kit (Sigma-Aldrich).

Glucose and insulin determination. Animals were fasted for 16 h overnight before blood was obtained from the tail vein. Glucose levels were determined using a standard glucometer. Insulin levels were analyzed using an insulin ELISA kit (Crystal Chem).

Glucose and insulin tolerance tests. Animals were fasted for 16 h and 6 h before i.p. injection of 2 g/kg glucose and 0.8 U/kg insulin, respectively. Blood was obtained at intervals of 15 minutes from the tail vein, and glucose and insulin levels were analyzed as described above.

Hyperinsulinemic, euglycemic clamps. Mice were kept on a high-fat diet for 3 weeks. Six days before the experiment, an indwelling catheter was implanted into the left jugular vein. After an overnight fast, 3-[^{3}H]-glucose (HPLC-purified; Perkin Elmer) was infused at a rate of 0.05 mCi/min for 2 h to assess the basal glucose turnover. Subsequently, hyperinsulinemic, euglycemic clamps were performed for 120 min with a primed and continuous infusion of insulin (126 pmol/kg primed, 18 pmol/kg/min infusion), and 20% dextrose was infused at variable rates to maintain plasma glucose at basal concentration (around 6.7 mM). To estimate insulin-stimulated whole-body fluxes, 3-[^{3}H]-glucose was infused at a rate of 0.1 mCi/min

throughout the clamps, and deoxy-D-[1-^{14}C]-glucose (Perkin Elmer) was injected as a bolus at minute 75 of the clamp to estimate the rate of insulin-stimulated tissue glucose uptake as previously described (51).

Determination of PI3K and Akt activity. Tissue (50 mg) was homogenized using a polytron at half-maximum speed for 1 min on ice in 500 μl buffer A (20 mM Tris, pH 7.5; 5 mM EDTA; 10 mM $Na_4P_2O_7$; 100 mM NaF; and 2 mM Na_3VO_4) containing 1% NP-40, 1 mM PMSF, 10 μg/ml aprotinin, and 10 μg/ml leupeptin. Tissue lysates were solubilized by continuous stirring for 1 h at 4°C and centrifuged for 10 min at 14,000 *g*. The supernatants were stored at –80°C until analysis. Tissue lysates (500 μg protein) were subjected to immunoprecipitation for 4 h at 4°C with 2 μg of a polyclonal IRS-1 antibody (Upstate Biotechnology), 2 μg of a polyclonal IRS-2 antibody (Upstate Biotechnology), or 2 μg of Akt antibody that recognizes both Akt1 and Akt2 (Upstate Biotechnology), coupled to protein A–Sepharose (Sigma-Aldrich) or protein G–Sepharose beads. The immune complex was washed, and PI3K and Akt activity was determined as described previously (52).

Islet morphology and immunohistochemistry. The pancreas was removed, fixed in 4% paraformaldehyde, and embedded in paraffin. Sections were stained for insulin, glucagon, and somatostatin, whereby insulin was detected by AMCA, glucagon by Texas red, and somatostatin by Cy2-conjugated secondary antibodies. The slides were mounted using antifade mounting media.

Evaluation of β cell and islet size. Pancreas sections from control mice or MKOs (n = 3) were immunostained with immunofluorescent anti-insulin and anti–β-catenin antibodies using standard protocols (53). The images of at least 6 randomly chosen islets from each section were captured, and the area of islets and β cells were measured using NIH ImageJ software (http://rsb.info.nih.gov/nih-image/). The number of insulin-positive β cells in each islet was identified by the nuclei stained with DAPI, and the relative density of β cells in islets was calculated as the number of β cell cells divided by islet size. The cellular area outlined by cell membrane stained for β-catenin was measured as the size of individual cells. The size of β cells was measured in at least 510 β cells from different islets in each mouse (using at least 3 different mice per group), and the mean ± SEM was calculated for each group. Mass of β cells was assessed in sections stained with a cocktail of antibodies against non–β cells (glucagon, somatostain, and pancreatic polypeptide) and calculated as described previously (54).

Histology. Tissues were dissected, embedded in OCT compound (Sakura Finetek), dehydrated, embedded in paraffin, and sectioned. The sections were subsequently stained for Cox activity and for SDH activity. Mononuclear infiltrates were quantified in H&E-stained sections by comparing the mean percent area occupied by mononucleated cells.

Islet isolation, DNA and insulin content determination, and glucose-stimulated insulin secretion. Islets were isolated by using collagenase digestion followed by separation using a density gradient, as previously described in detail (55). After isolation, the islets were handpicked and cultured overnight in RPMI 1640 containing 7 mM glucose and supplemented with 10% fetal bovine serum. Total insulin and DNA content of the isolated islets was measured after sonication of the islet sample in ddH_2O. Each sample was split in equal aliquots, and 1 aliquot per sample was stored at –20°C for analysis of DNA content. Insulin content was determined in the remaining aliquot by extraction in acid ethanol overnight. Samples were diluted appropriately, and insulin content was measured by radioimmunoassay (Linco Research Inc.) with rat insulin as standard. DNA was measured using the CyQuant cell proliferation assay kit (Invitrogen) and quantified by use of a spectrofluorometer.

Insulin release was studied in isolated islets after overnight culture. Briefly, groups of 20 islets were placed in medium contain low glucose (3.3 mM) for 30 min at 37°C. After this preincubation, the medium was removed, and fresh medium containing 3.3 mM glucose was added. The islets were incubated at 37°C for 60 min, and medium samples were stored at –20°C. Fresh medium containing 16.7 mM glucose was added before additional incubation for 60 min at 37°C. The medium was then removed, and insulin content in media samples was measure by radioimmunoassay. The remaining islets were collected, washed in PBS, and used for RNA and genomic DNA isolation.

IL-6 treatment and hormone secretion analysis of islets. Islets were obtained by collagenase digestion as previously described (53) and were maintained in the RPMI 1640 media supplemented with 7 mM glucose. After incubating in the RPMI media overnight, the islets were treated with or without 400 pg/ml IL-6 for 24 h. Batches of 10 isolated islets were preincubated for 30 min at 37°C in 500 μl of 10 mM HEPES–balanced Krebs Ringer bicarbonate buffer (KRBB; 129 mM NaCl, 5 mM $NaHCO_3$, 4.8 mM KCl, 1.2 mM KH_2PO_4, 1.2 mM $MgSO_4$, 10 mM HEPES, and 2.5 mM $CaCl_2$ at pH 7.4) supplemented with 3.3 mM glucose and 0.1 % BSA. Islets were centrifuged briefly, and the supernatant was collected for basal insulin secretion. Islets were then incubated for 1 h at 37°C in 500 μl KRBB with 0.1% BSA containing different glucose and/or additives as indicated. Islets were centrifuged briefly, and the supernatant was collected for stimulated insulin secretion. Then relative insulin secretion was calculated as the incubation/preincubation ratio. The insulin was measured by radioimmunoassay.

Serum IL-6 determination. IL-6 was determined from mouse serum or from conditioned medium of muscle cells in culture using the Quantikine Mouse IL-6 ELISA kit according to the manufacturer's instructions (R&D Systems).

Linear regression analysis. Collection of gene expression data and clinical variables from 42 human volunteers has been published previously, including 17 individuals with normal glucose tolerance (7). We used our previously published normalized gene expression data from human skeletal muscle (7). Expression of PGC-1α (*PPARGC1A)* was deviated in one sample (identification no. 10519) compared with all others; hence, we excluded data from this sample for further analysis. We performed multiple-regression analysis to predict the variance in *IL-6* or *TNF*-α expression, considered as dependent variables, based on BMI, fasting glucose (log transformed), and fasting insulin (log transformed), considered as independent variables.

Statistics. All statistical analyses were performed using Number Cruncher Statistical Systems software (NCSS). All results are expressed as mean ± SEM. Statistical significance was determined by 2-tailed Student's t test. A P value less than 0.05 was considered significant.

Acknowledgments

The authors thank Eleftheria Maratos-Flier and Fen-Fen Liu (Beth Israel Deaconess Medical Center) for help with the indirect calorimetry (CLAMS) experiments. C. Handschin is supported by a Scientist Career Development Grant of the Muscular Dystrophy Association, the Swiss National Science Foundation Professorship PP00A-110746, and the University Research Priority Program "Integrative Human Physiology" of the University of Zurich. The work described in this article is supported by NIH grants DK54477 and DK61562 to B.M. Spiegelman. G.I. Shulman is supported by NIH grants RO1 DK-40936 and U24 DK-59635 and by a Distinguished Clinical Scientist Award from the American Diabetes Association. R.N. Kulkarni is supported by NIH grant RO1 DK-67536 and the Ernst Oppenheimer Award from the Endocrine Society. D. Kawamori is the recipient of a research fellowship from the Manpei Suzuki Diabetes Foundation (Tokyo, Japan).

Received for publication February 12, 2007, and accepted in revised form July 17, 2007.

Address correspondence to: Bruce M. Spiegelman, Dana-Farber Cancer Institute, Smith Building, One Jimmy Fund Way, Boston, Massachusetts 02115, USA. Phone: (617) 632-3567; Fax: (617) 632-4655; E-mail: bruce_spiegelman@dfci.harvard.edu.

1. Handschin, C., and Spiegelman, B.M. 2006. PGC-1 coactivators, energy homeostasis, and metabolism. *Endocr. Rev.* **27**:728–735.
2. Lin, J., Handschin, C., and Spiegelman, B.M. 2005. Metabolic control through the PGC-1 family of transcription coactivators. *Cell Metab.* **1**:361–370.
3. Wu, Z., et al. 1999. Mechanisms controlling mitochondrial biogenesis and respiration through the thermogenic coactivator PGC-1. *Cell.* **98**:115–124.
4. Lin, J., et al. 2002. Transcriptional co-activator PGC-1 alpha drives the formation of slow-twitch muscle fibres. *Nature.* **418**:797–801.
5. Yoon, J.C., et al. 2001. Control of hepatic gluconeogenesis through the transcriptional coactivator PGC-1. *Nature.* **413**:131–138.
6. Yoon, J.C., et al. 2003. Suppression of beta cell energy metabolism and insulin release by PGC-1alpha. *Dev. Cell.* **5**:73–83.
7. Mootha, V.K., et al. 2003. PGC-1alpha-responsive genes involved in oxidative phosphorylation are coordinately downregulated in human diabetes. *Nat. Genet.* **34**:267–273.
8. Patti, M.E., et al. 2003. Coordinated reduction of genes of oxidative metabolism in humans with insulin resistance and diabetes: Potential role of PGC1 and NRF1. *Proc. Natl. Acad. Sci. U. S. A.* **100**:8466–8471.
9. Mootha, V.K., et al. 2004. Erralpha and Gabpa/b specify PGC-1alpha-dependent oxidative phosphorylation gene expression that is altered in diabetic muscle. *Proc. Natl. Acad. Sci. U. S. A.* **101**:6570–6575.
10. Schreiber, S.N., et al. 2004. The estrogen-related receptor alpha (ERRalpha) functions in PPARgamma coactivator 1alpha (PGC-1alpha)-induced mitochondrial biogenesis. *Proc. Natl. Acad. Sci. U. S. A.* **101**:6472–6477.
11. Handschin, C., Rhee, J., Lin, J., Tarr, P.T., and Spiegelman, B.M. 2003. An autoregulatory loop controls peroxisome proliferator-activated receptor gamma coactivator 1alpha expression in muscle. *Proc. Natl. Acad. Sci. U. S. A.* **100**:7111–7116.
12. Czubryt, M.P., McAnally, J., Fishman, G.I., and Olson, E.N. 2003. Regulation of peroxisome proliferator-activated receptor gamma coactivator 1alpha (PGC-1alpha) and mitochondrial function by MEF2 and HDAC5. *Proc. Natl. Acad. Sci. U. S. A.* **100**:1711–1716.
13. Handschin, C., and Mootha, V.K. 2005. Estrogen-related receptor α (ERRα): A novel target in type 2 diabetes. *Drug Discovery Today: Therapeutic Strategies.* **2**:151–156.
14. Petersen, K.F., Dufour, S., and Shulman, G.I. 2005. Decreased insulin-stimulated ATP synthesis and phosphate transport in muscle of insulin-resistant offspring of type 2 diabetic parents. *PLoS Med.* **2**:e233.
15. Petersen, K.F., Dufour, S., Befroy, D., Garcia, R., and Shulman, G.I. 2004. Impaired mitochondrial activity in the insulin-resistant offspring of patients with type 2 diabetes. *N. Engl. J. Med.* **350**:664–671.
16. Petersen, K.F., et al. 2003. Mitochondrial dysfunction in the elderly: possible role in insulin resistance. *Science.* **300**:1140–1142.
17. Lin, J., et al. 2004. Defects in adaptive energy metabolism with CNS-linked hyperactivity in PGC-1alpha null mice. *Cell.* **119**:121–135.
18. Leone, T.C., et al. 2005. PGC-1alpha deficiency causes multi-system energy metabolic derangements: muscle dysfunction, abnormal weight control and hepatic steatosis. *PLoS Biol.* **3**:e101.
19. Handschin, C., et al. 2005. Nutritional regulation of hepatic heme biosynthesis and porphyria through PGC-1alpha. *Cell.* **122**:505–515.
20. Li, S., et al. 2005. Requirement for serum response factor for skeletal muscle growth and maturation revealed by tissue-specific gene deletion in mice. *Proc. Natl. Acad. Sci. U. S. A.* **102**:1082–1087.
21. Handschin, C., et al. 2007. Skeletal muscle fiber-type switching, exercise intolerance and myopathy in PGC-1alpha muscle-specific knockout animals. *J. Biol. Chem.* doi:10.1074/jbc.M704817200.
22. Michael, L.F., et al. 2001. Restoration of insulin-sensitive glucose transporter (GLUT4) gene expression in muscle cells by the transcriptional coactivator PGC-1. *Proc. Natl. Acad. Sci. U. S. A.* **98**:3820–3825.
23. Chiasson, J.L., and Rabasa-Lhoret, R. 2004. Prevention of type 2 diabetes: insulin resistance and beta-cell function. *Diabetes.* **53**(Suppl. 3):S34–S38.
24. Nawrocki, A.R., and Scherer, P.E. 2004. The delicate balance between fat and muscle: adipokines in metabolic disease and musculoskeletal inflammation. *Curr. Opin. Pharmacol.* **4**:281–289.
25. Trayhurn, P., Bing, C., and Wood, I.S. 2006. Adipose tissue and adipokines — energy regulation from the human perspective. *J. Nutr.* **136**:1935S–1939S.
26. Pedersen, B.K., et al. 2003. Searching for the exercise factor: is IL-6 a candidate? *J. Muscle Res. Cell Motil.* **24**:113–119.
27. Boden, G. 2006. Fatty acid-induced inflammation and insulin resistance in skeletal muscle and liver. *Curr. Diab. Rep.* **6**:177–181.
28. Brake, D.K., Smith, E.O., Mersmann, H., Smith, C.W., and Robker, R.L. 2006. ICAM-1 expression in adipose tissue: effects of diet-induced obesity in mice. *Am. J. Physiol. Cell Physiol.* **291**:C1232–C1239.
29. Kosmidou, I., et al. 2002. Production of interleukin-6 by skeletal myotubes: role of reactive oxygen species. *Am. J. Respir. Cell Mol. Biol.* **26**:587–593.
30. St-Pierre, J., et al. 2006. Suppression of reactive oxygen species and neurodegeneration by the PGC-1 transcriptional coactivators. *Cell.* **127**:397–408.
31. Sparks, L.M., et al. 2005. A high-fat diet coordinately downregulates genes required for mitochondrial oxidative phosphorylation in skeletal muscle. *Diabetes.* **54**:1926–1933.
32. Vianna, C.R., et al. 2006. Hypomorphic mutation of PGC-1beta causes mitochondrial dysfunction and liver insulin resistance. *Cell Metab.* **4**:453–464.
33. Kristiansen, O.P., and Mandrup-Poulsen, T. 2005. Interleukin-6 and diabetes: the good, the bad, or the indifferent? *Diabetes.* **54**(Suppl. 2):S114–S124.
34. Southern, C., Schulster, D., and Green, I.C. 1990. Inhibition of insulin secretion from rat islets of Langerhans by interleukin-6. An effect distinct from that of interleukin-1. *Biochem. J.* **272**:243–245.
35. Sandler, S., Bendtzen, K., Eizirik, D.L., and Welsh, M. 1990. Interleukin-6 affects insulin secretion and glucose metabolism of rat pancreatic islets in vitro. *Endocrinology.* **126**:1288–1294.
36. Rotter Sopasakis, V., Larsson, B.M., Johansson, A., Holmang, A., and Smith, U. 2004. Short-term infusion of interleukin-6 does not induce insulin resistance in vivo or impair insulin signalling in rats. *Diabetologia.* **47**:1879–1887.
37. Alexandraki, K., et al. 2006. Inflammatory process in type 2 diabetes: the role of cytokines. *Ann. N. Y. Acad. Sci.* **1084**:89–117.
38. Youd, J.M., Rattigan, S., and Clark, M.G. 2000. Acute impairment of insulin-mediated capillary recruitment and glucose uptake in rat skeletal muscle in vivo by TNF-alpha. *Diabetes.* **49**:1904–1909.
39. Maedler, K., et al. 2006. Low concentration of interleukin-1beta induces FLICE-inhibitory protein-mediated beta-cell proliferation in human pancreatic islets. *Diabetes.* **55**:2713–2722.
40. Busquets, S., Figueras, M., Almendro, V., Lopez-Soriano, F.J., and Argiles, J.M. 2006. Interleukin-15 increases glucose uptake in skeletal muscle. An antidiabetogenic effect of the cytokine. *Biochim. Biophys. Acta.* **1760**:1613–1617.
41. Larsen, C.M., et al. 2007. Interleukin-1-receptor antagonist in type 2 diabetes mellitus. *N. Engl. J. Med.* **356**:1517–1526.
42. Pedersen, B.K., and Fischer, C.P. 2007. Physiological roles of muscle-derived interleukin-6 in response to exercise. *Curr. Opin. Clin. Nutr. Metab. Care.* **10**:265–271.
43. Borniquel, S., Valle, I., Cadenas, S., Lamas, S., and Monsalve, M. 2006. Nitric oxide regulates mitochondrial oxidative stress protection via the transcriptional coactivator PGC-1alpha. *FASEB J.* **20**:1889–1891.
44. Valle, I., Alvarez-Barrientos, A., Arza, E., Lamas, S., and Monsalve, M. 2005. PGC-1alpha regulates the mitochondrial antioxidant defense system in vascular endothelial cells. *Cardiovasc. Res.* **66**:562–573.
45. Vats, D., et al. 2006. Oxidative metabolism and PGC-1beta attenuate macrophage-mediated inflammation. *Cell Metab.* **4**:13–24.
46. Vasudevan, A.R., Burns, A., and Fonseca, V.A. 2006. The effectiveness of intensive glycemic control for the prevention of vascular complications in diabetes mellitus. *Treat. Endocrinol.* **5**:273–286.
47. Butler, A.E., et al. 2003. Beta-cell deficit and increased beta-cell apoptosis in humans with type 2 diabetes. *Diabetes.* **52**:102–110.
48. Sandri, M., et al. 2006. PGC-1{alpha} protects skeletal muscle from atrophy by suppressing FoxO3 action and atrophy-specific gene transcription. *Proc. Natl. Acad. Sci. U. S. A.* **103**:16260–16265.
49. Arany, Z., et al. 2005. Transcriptional coactivator PGC-1 alpha controls the energy state and contractile function of cardiac muscle. *Cell Metab.* **1**:259–271.
50. Puigserver, P., et al. 1999. Activation of PPARgamma coactivator-1 through transcription factor docking. *Science.* **286**:1368–1371.
51. Samuel, V.T., et al. 2006. Targeting foxo1 in mice using antisense oligonucleotide improves hepatic and peripheral insulin action. *Diabetes.* **55**:2042–2050.
52. Kim, Y.B., Shulman, G.I., and Kahn, B.B. 2002. Fatty acid infusion selectively impairs insulin action on Akt1 and protein kinase C lambda /zeta but not on glycogen synthase kinase-3. *J. Biol. Chem.* **277**:32915–32922.
53. Kulkarni, R.N., et al. 1999. Tissue-specific knockout of the insulin receptor in pancreatic beta cells creates an insulin secretory defect similar to that in type 2 diabetes. *Cell.* **96**:329–339.
54. Kulkarni, R.N., et al. 1999. Altered function of insulin receptor substrate-1-deficient mouse islets and cultured beta-cell lines. *J. Clin. Invest.* **104**:R69–R75.
55. Gotoh, M., et al. 1985. An improved method for isolation of mouse pancreatic islets. *Transplantation.* **40**:437–438.